Synergistic effect of Fano resonance and optical nonlinearity in laser trapping of silver nanoparticles

Sumit Yadav,[1] Anita Devi,[1] and Arijit K. De[2,*]

[1]*Department of Physical Sciences, Indian Institute of Science Education and Research (IISER) Mohali, Knowledge City, Sector 81, SAS Nagar, Punjab 140306, India*

[2]*Department of Chemical Sciences, Indian Institute of Science Education and Research (IISER) Mohali, Knowledge City, Sector 81, SAS Nagar, Punjab 140306, India*

(Received 10 May 2020; accepted 10 September 2020; published 13 October 2020)

Optical trapping efficiency for silver nanoparticles is theoretically estimated using dipole approximation and generalized Lorenz-Mie theory, including higher-order optical nonlinear effects. Here, we show a reversal in asymmetry of axial trapping potential due to Fano resonance is observed, along with a splitting of trapping potential well due to optical nonlinearity. Further, it is shown that there exists a limit for particle size beyond which the particle cannot be trapped and how this limit can be extended by harnessing optical nonlinearity under femtosecond pulsed excitation.

DOI: 10.1103/PhysRevA.102.043511

I. INTRODUCTION:

To achieve precise translation and rotational control at nanoscale in a noninvasive way, trapping and manipulation of nanoparticles was achieved by utilizing radiation pressure in an optical tweezers [1–3]. Of special interest has been to optically trap metallic nanoparticles which are efficient probes for nanotechnology and biomedical applications. Compared with dielectrics, the enhanced polarizability of metals (due to the presence of free electrons) was shown to facilitate trapping of metallic nanoparticles [4–8]. However, a major challenge to facile optical trapping is posed by the enhanced reflectivity with increasing particle size, restricting the maximum size of the particle to be trapped [6]. One puzzling observation for silver nanoparticles was that the trapping efficiency was found to be strongly dependent on particle size; for smaller nanoparticles ($\leqslant$20 nm), very high laser power was required to circumvent the erratic Brownian motion, and use of pulsed excitation, instead of conventional continuous-wave (cw) excitation, was proposed [6]. Under pulsed-excitation, nonlinear optical effects are expected to contribute significantly, particularly when the peak intensity is quite high, for example, under high repetition-rate femtosecond pulsed excitation, which has recently been shown for both dielectric [9–11] and metallic [12,13] nanoparticles. Intrigued by these fascinating aspects for optical trapping of silver nanoparticles, in this paper we extend our preliminary theoretical studies [14] to investigate the interference effects (under both cw and pulsed excitations) including higher-order nonlinear optical effects (under pulsed excitation).

II. METHOD

We compare and contrast force and potential numerically simulate using both dipole approximation [15] with that obtained from generalized Lorenz-Mie theory (GLMT) [16–19] for silver nanoparticles. The force expression corresponding to GLMT (using a localized approximation) for an on-axis particle can be expressed as

$$F_{\text{axial}}^{\text{GLMT}}(z;\ r=0) = \left(\frac{n^w}{c}\right)\left(\frac{2P_{\text{peak/avg}}}{\pi w_0^2}\right)C_n^{pr}(z), \tag{1}$$

where n^w is the refractive index of surrounding medium (water), c is the speed of light, $w_0 = 0.82(\lambda/NA)$ is the spot size (i.e., Gaussian beam radius at focus) where NA is numerical aperture, λ is the wavelength of trapping beam, $P_{\text{peak/avg}}$ is the average power for cw excitation or peak power for pulsed excitation, and $C_n^{pr}(z)$ is the pressure cross section given by

$$C_n^{pr}(z) = \left(\frac{\lambda^2}{2\pi}\right)\sum_n\left[\left(\frac{2n+1}{n(n+1)}\right)|g_n|^2 S_n^{(1)} + \left(\frac{n(n+2)}{n+1}\right)\text{Re}\left[g_n g_{n+1}^* S_n^{(2)}\right]\right], \tag{2}$$

where $S_n^{(1)}$ and $S_n^{(2)}$ are scattering coefficients, and g_n are beam shaping coefficient (BSC). For a Gaussian beam profile using localized approximation, it can be expressed as

$$g_n = iQ\exp\left[-iQ\left(\frac{\rho_n}{w_0}\right)^2\right]e^{ikz_0}, \tag{3}$$

where $Q = \frac{1}{i+2\frac{z-z_0}{l}}$, z is the axial position, z_0 is the axial position of focus that we took as zero for simplicity, $l = kw_0^2$ is spreading length, $k = 2\pi(n^w/\lambda)$ is wave vector inside water, and $\rho_n = (\frac{n+1/2}{2\pi})\lambda$. Here, $S_n^{(1)}$ and $S_n^{(2)}$ are the function of Mie scattering coefficients (MSCs), which can be written as [19,20]

$$S_n^{(1)} = \text{Re}(a_n + b_n - 2a_n b_n^*), \tag{4a}$$

$$S_n^{(2)} = (a_n + b_n + a_{n+1} + b_{n+1} - 2a_n a_{n+1}^* - 2b_n b_{n+1}^*), \tag{4b}$$

$$a_n = \left(\frac{\psi_n(\alpha)\psi'_n(\beta) - M\psi'_n(\alpha)\psi_n(\beta)}{\xi_n(\alpha)\psi'_n(\beta) - M\xi'_n(\alpha)\psi_n(\beta)}\right), \tag{5a}$$

$$b_n = \left(\frac{M\psi_n(\alpha)\psi'_n(\beta) - \psi'_n(\alpha)\psi_n(\beta)}{M\xi_n(\alpha)\psi'_n(\beta) - \xi'_n(\alpha)\psi_n(\beta)}\right), \tag{5b}$$

*akde@iisermohali.ac.in

 ©2020 American Physical Society

TABLE I. List of the parameters used in numerical calculations.

Parameters	Value
λ	800 nm
c	3×10^8 m/s
f	76 MHz
τ	120 fs
NA	1.4
ε_∞	2.5 [20]
ω_p	1.37×10^{16} Hz [20]
γ_c	3.2258×10^{13} Hz [20]
n_0^w	1.329 [9]
n_2^w	2.7×10^{-20} m^2/W [27]
n_2^s	7.5×10^{-20} m^2/W [28]
n_4^s	5×10^{-35} m^4/W^2 [28]
n_6^s	7.5×10^{-51} m^6/W^3 [28]
σ_2^s	13.2×10^{-14} m/W [28]
σ_4^s	9×10^{-29} m^3/W^2 [28]
σ_6^s	7×10^{-44} m^5/W^3 [28]

where $\alpha = kr$ or $\beta = M\alpha$, where $r = d/2$ is the radius of trap particle, ψ_n are spherical Bessel function of positive and negative half integer, ξ_n are Ricatti-Bessel functions, and $M = n^s/n^w$ is the relative refractive index (RI) of the particle to that of the medium. Please note that unlike dielectrics, for metals the imaginary part of the RI (leading to absorptive force) also contributes significantly. Therefore, the total RI of silver particles can be written as $n^s = n_0^s + i\kappa_0^s$; here, n_0^s and κ_0^s are the linear RI, and linear extinction coefficient ($\kappa = \frac{\sigma\lambda}{4\pi}$) of the silver nanoparticles, which is defined in terms of absorption coefficients (σ). Accordingly, relative RI value is also complex wherefore, ψ_n and ξ_n values are complex, and corresponding MSCs are also determined in complex value. For RI calculation, $n_0^s = \sqrt{\frac{\epsilon_1}{2} + \frac{\sqrt{\epsilon_1^2+\epsilon_2^2}}{2}}$ is the real linear part of RI and $\kappa_0^s = \frac{\epsilon_2}{2n_0^s}$ is the imaginary linear part, which corresponds to the absorptivity; here, $\epsilon_1 = \mathrm{Re}[\epsilon]$, $\epsilon_2 = \mathrm{Im}[\epsilon]$ and the electric permittivity of metals can be written as $\epsilon = \varepsilon_\infty - \frac{\omega_p^2}{\omega^2 + i\gamma_c\omega}$ according to the corrected Drude-Lorentz model [20], where, ε_∞ is the background permittivity, ω_p is the plasma frequency, γ_c is the collision damping frequency, and $\omega = \frac{2\pi c}{\lambda}$ is the natural frequency. Under dipole approximation, the force expressions are expressed as [15]

$$\begin{aligned} F_{\mathrm{axial}}^{\mathrm{dipole}}(z; r=0) &= -\frac{2\pi n^w r^3}{c}\mathrm{Re}[\alpha_0]\frac{8Z/(kw_0^2)}{(1+4Z^2)^2}\frac{2P_{\mathrm{peak/avg}}}{\pi w_0^2} \\ &+ \frac{8\pi n^w k^4 r^6}{3c}|\alpha_0|^2\frac{2P_{\mathrm{peak/avg}}}{\pi w_0^2(1+4Z^2)} \\ &+ \frac{4k\pi n^w r^3}{c}\mathrm{Im}[\alpha_0]\frac{2P_{\mathrm{peak/avg}}}{\pi w_0^2(1+4Z^2)}, \end{aligned} \tag{6}$$

where $Z = \frac{z}{kw_0^2}$ is the reduced coordinate and $\alpha_0 = (\frac{M^2-1}{M^2+2})$ is polarizability per unit volume. Under cw excitation optical nonlinearity can be ignored; therefore, the total RIs for particle and the surrounding medium are:

$$n^{s/w} \approx n_0^{s/w}. \tag{7a}$$

Under pulsed excitation, nonlinear effects (beyond optical Kerr effect, OKE) are significant and the total RI for particle is

$$\begin{aligned} n^s = n_0^s + n_2^s I_{\mathrm{peak}} + n_4^s I_{\mathrm{peak}}^2 + n_6^s I_{\mathrm{peak}}^3 \\ + i\left(\kappa_0^s + \kappa_2^s I_{\mathrm{peak}} + \kappa_4^s I_{\mathrm{peak}}^2 + \kappa_6^s I_{\mathrm{peak}}^3\right), \end{aligned} \tag{7b}$$

where n_2^s, n_4^s, n_6^s, are, respectively, the second, fourth, and sixth-order nonlinear RI; κ_2^s, κ_4^s, and κ_6^s are the second, fourth, and sixth-order nonlinear extinction coefficients. For the surrounding medium (water), nonlinear RI does not contribute significantly; therefore, it can be ignored (i.e., $n^w \approx n_0^w$). For a focused Gaussian beam, the on-axis intensity can be expressed as

$$I_{\mathrm{peak/avg}}(z; r=0) = \left(\frac{2P_{\mathrm{peak/avg}}}{\pi w_0^2}\right)\frac{1}{1+(2Z)^2}. \tag{8}$$

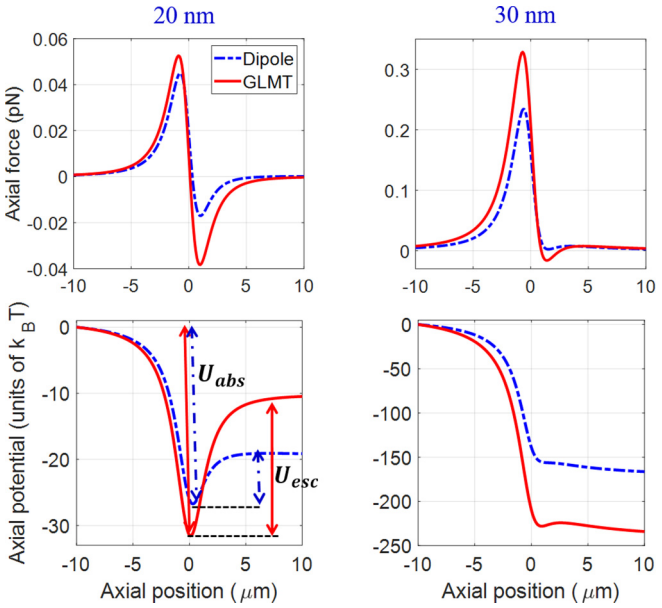

FIG. 1. Plots of trapping force or potential using dipole approximation and GLMT at 100-mW average power under cw excitation.

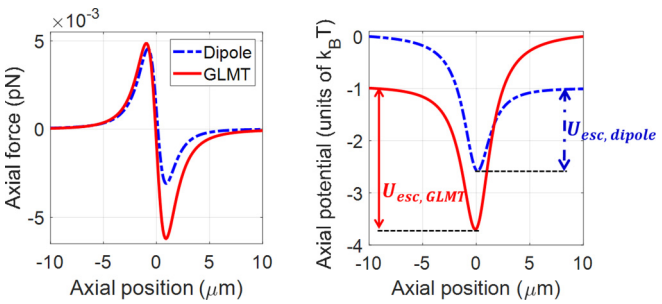

FIG. 2. Plots of trapping force or potential using dipole approximation and GLMT at 100-mW average power for 10-nm particle under cw excitation.

TABLE II. Numerical values of the scattering coefficient at 100-mW average power under cw excitation.

Coefficients	10 nm	20 nm
$S_n^{(1)}$	-3.58×10^{-6}	38.93×10^{-6}
$S_n^{(2)}$	$-3.59 \times 10^{-6} + 0.001i$	$37.01 \times 10^{-6} + 0.008i$
a_1	$-3.55 \times 10^{-6} + 0.001i$	$38.27 \times 10^{-6} + 0.005i$
b_1	$-0.03 \times 10^{-6} - 2.83 \times 10^{-6}i$	$-0.88 \times 10^{-6} - 87.41 \times 10^{-6}i$

Under cw excitation, the force is calculated for GLMT and dipole approximation using Eqs. (1) and (6), respectively, and the potential is calculated by numerically integrating the corresponding forces. However, under pulsed excitation, the force is calculated by a time averaging of instantaneous force over one duty cycle using (for details, see Ref. [9])

$$\langle F_{\text{pulsed}} \rangle = \frac{1}{T} \int_{-\tau/2}^{\tau/2} F_{\text{pulsed}} dt, \tag{9}$$

where τ is the pulse width and T is the inverse of repetition rate. The parameters used in the numerical calculations are according to the commercially available Ti:sapphire femtosecond oscillator. All the parameters used in the simulations are mentioned in Table I.

III. RESULTS AND DISCUSSION

In the figures to follow, the solid red curve corresponds to GLMT results and the dotted blue curve corresponds to dipole approximation results (unless otherwise mentioned). Due to simultaneous action of (axial component of) gradient force and scattering force, the axial trapping potential is always asymmetric (which positions the minimum of potential slightly ahead of the geometric focus) and it is more likely that a trapped particle always escapes in the forward direction by crossing the lower potential barrier lying ahead of the potential minimum. For dielectric nanoparticles, using dipole approximation, it was shown that this asymmetry increases significantly when OKE is included in numerical simulation, and height of the barrier (defined as *escape potential*, U_{esc}) is progressively reduced with an increase in laser power [9].

Figure 1 shows the trapping force and potential along the axial direction for 20- and 30-nm particle size at 100-mW average power under cw excitation. It can be seen that there is a significant enhancement in force and potential for GLMT results compared to dipole approximation results under similar conditions; for example for 20-nm particle, the escape potential for GLMT is $\sim 21\, k_B T$, but for dipole approximation it is $\sim 8\, k_B T$. GLMT shows approximately 2.7 times enhancement in trapping efficiency than dipole approximation for 20-nm particle size. However, for 30-nm particle size the escape potential using GLMT and dipole approximations are $\sim 4\, k_B T$ and $\sim 0\, k_B T$, respectively, which implies that according to GLMT, 30-nm particle can be trapped for a small duration but dipole approximation shows no stable trapping under similar conditions. Also, under cw excitation, force and potential is linearly proportional to power, therefore increasing power monotonically increases the escape potential for fixed particle size.

Quite interestingly, for particle size less than 15 nm, we observe a transition in the axial asymmetry, as shown in Fig. 2 for 10-nm particle size at 100-mW average power under cw excitation. It is observed that the escape potential is higher for GLMT than dipole approximation, which implies that GLMT estimates a better trapping efficiency than dipole approximation. However, dipole approximation result shows the location of barrier corresponding ahead of the potential minimum whereas for GLMT result it is located on the other side of the potential minimum.

We ascribe the origin of this change in axial asymmetry to MSCs (since BSCs are independent of particle size). From Table II, it can be seen that as we go from 10-nm particle

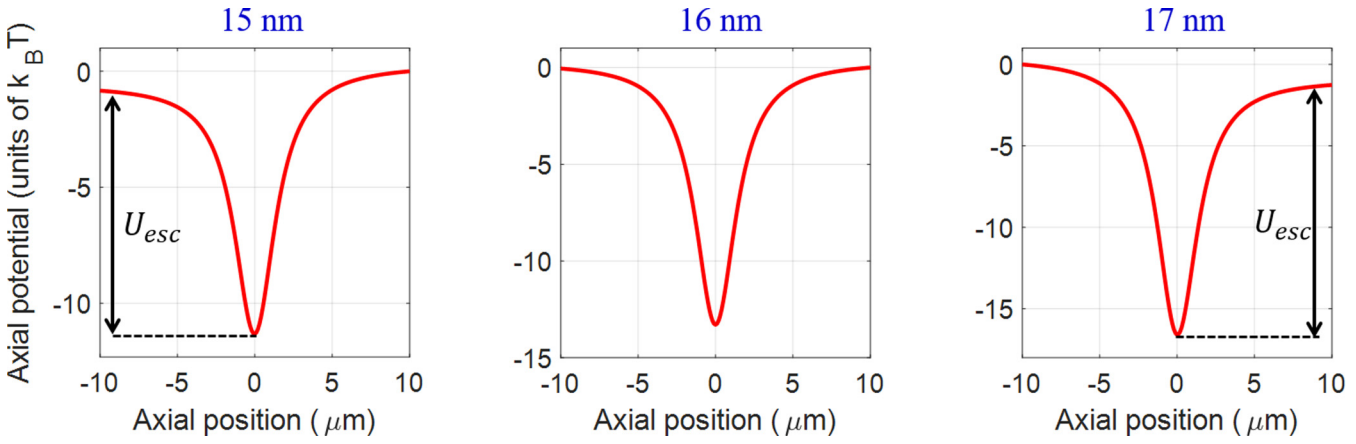

FIG. 3. Plots of trapping potential using GLMT at 100-mW average power under cw excitation.

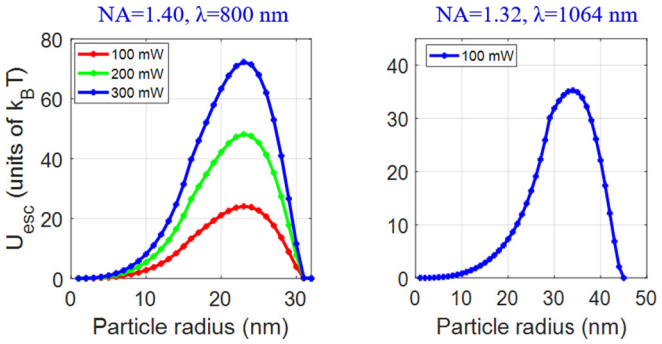

FIG. 4. Plots of escape potential against particle size using GLMT at 100-mW average power under cw excitation.

size to 20-nm particle size, there is a change in the sign of real component of $S_n^{(1)}$ and $S_n^{(2)}$ due to the change in sign of a_n, and it is well known that for smaller-size particle a_1 contributes significantly as compared to higher-order a_n coefficients. As a result, forward scattering is significantly enhanced over backward scattering, which leads to considerable attenuation of backward scattering force along the direction of light propagation and resulting in a net *negative optical scattering force* [21]. This phenomenon is known as *Fano resonance* [21–24], which appears in any medium due to the interference between scattering amplitude of resonance and background. Note that the MSCs can be written as a summation of narrow resonance and slow-varying background, which is equivalent to Fano profile [25,26]. This gradual transition in axial asymmetry with particle size at 100-mW average power under cw excitation is shown in Fig. 3. Interestingly, for ∼16 nm, particle size forward and backward scattering forces balance each other and results in the symmetric potential well.

For the chosen parameters listed in Table I, simulation results using GLMT show no stable trapping (i.e.,$U_{esc} = 0$) of particles having diameter beyond 31 nm, as shown in Fig 4 (the same using dipole approximation showed this limiting size to be 27 nm [13]). Note that this limiting size is unchanged even if we change laser power. In Fig. 4, we also show variation of U_{esc} with particle size for parameters used in earlier experiment [6], i.e., under 1064-nm cw excitation with NA = 1.32; the limiting particle size turns out to be 31 nm which is much smaller than that experimentally measured (137 nm). This led us to further investigate if the theoretical size limit could be extended by considering possible contributions from optical nonlinearity (which is expected to be significant particularly under pulsed excitation).

Figure 5 shows the trapping force and potential along the axial direction for 10-, 20-, and 30-nm particle size at 100-mW average power under pulsed excitation. A significant enhancement in the force and potential is observed for GLMT than for dipole approximation, which is reflected through the potential curve and can be quantified by escape potential. However, for a fixed average power (100 mW), the transition of axial asymmetry occurs at larger particle sizes under pulsed excitation as compared to cw excitation due to the significant contribution of nonlinearity under pulsed excitation. Also,

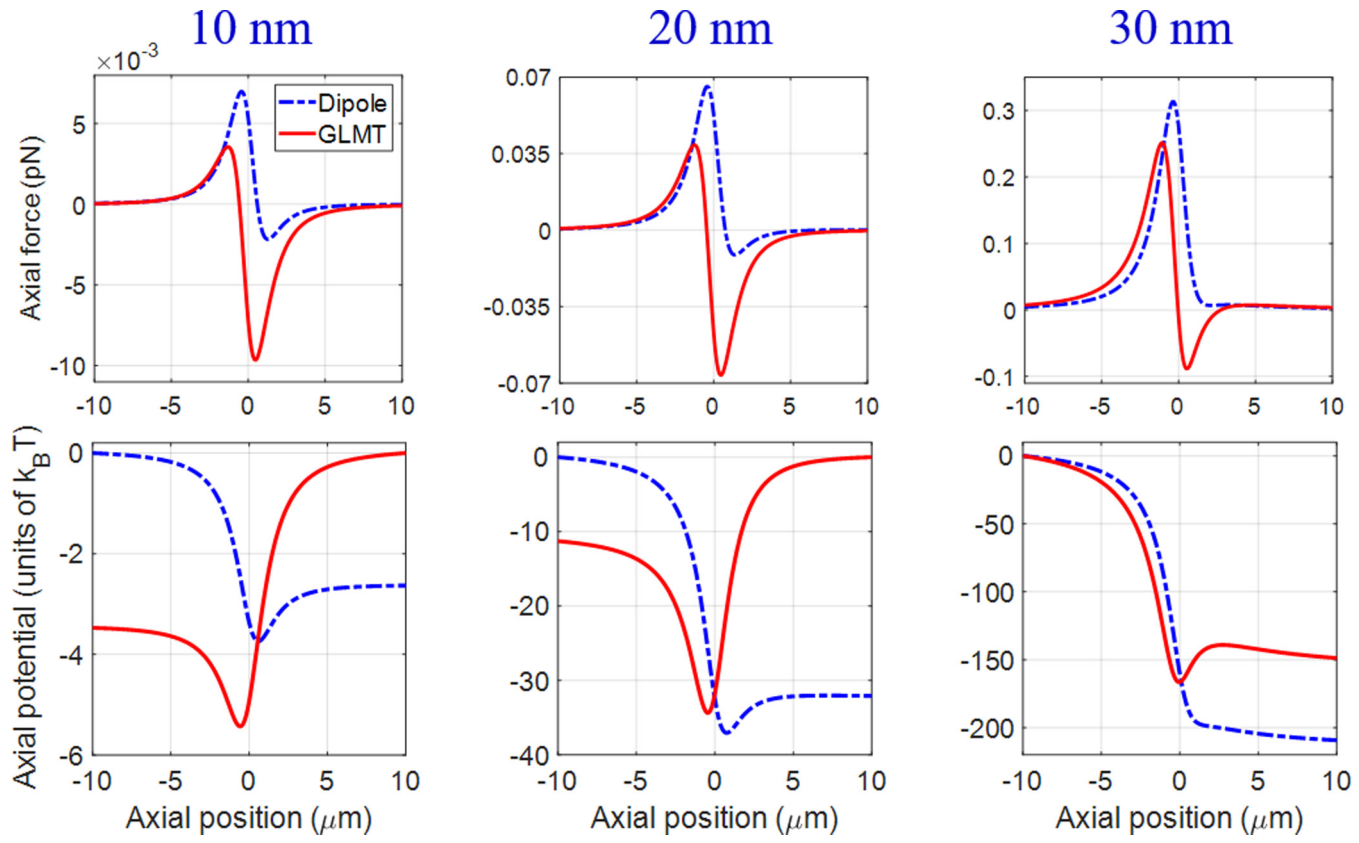

FIG. 5. Plots of trapping force or potential using GLMT and dipole approximation at 100-mW average power under pulsed excitation.

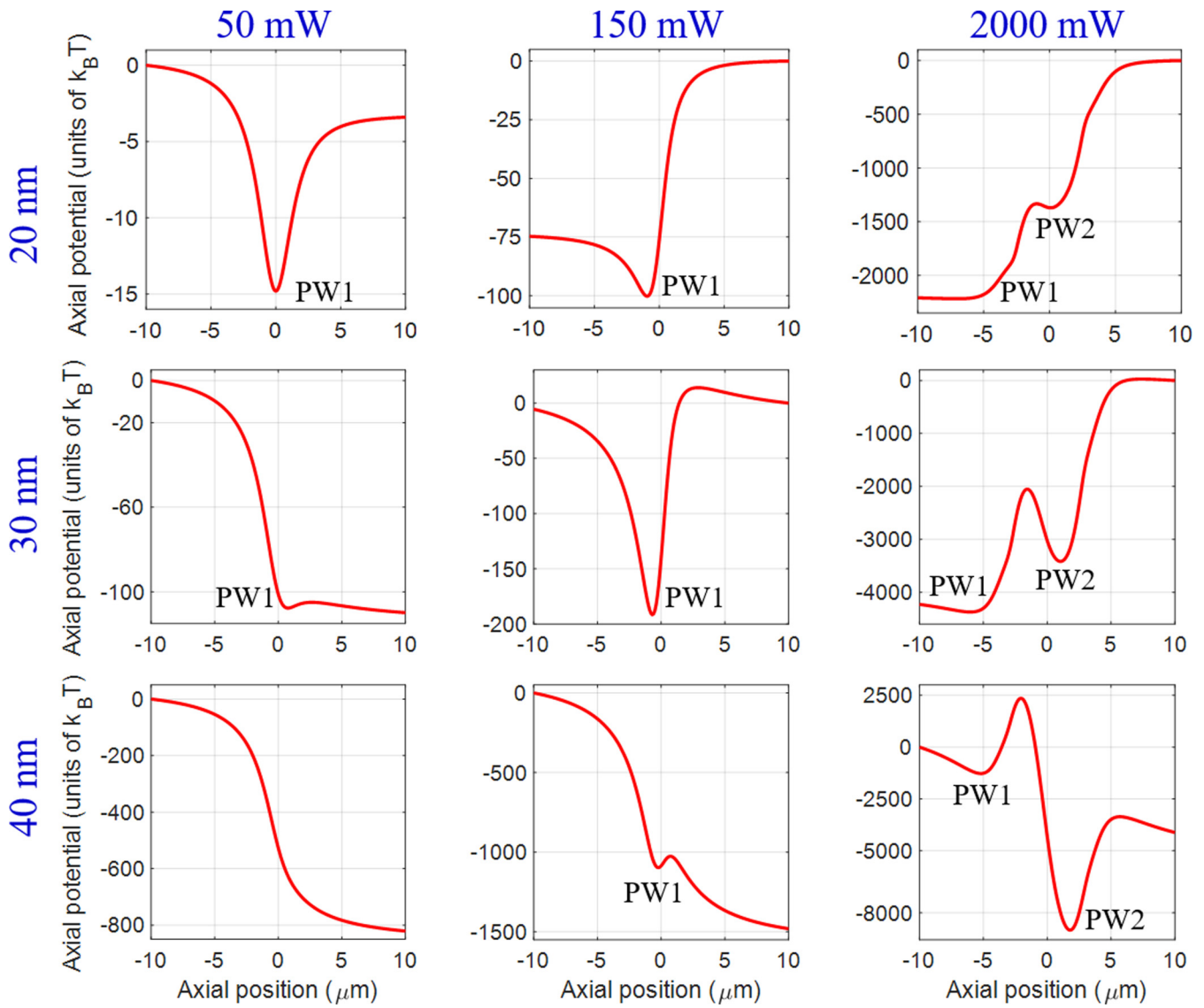

FIG. 6. Plots of trapping potential using GLMT under pulsed excitation.

30-nm particle shows a significantly enhanced (approximately 9 times) escape potential which implies that 30-nm particle can be stably trapped under pulsed excitation than cw excitation.

Further, we explore the effect of nonlinearity by varying the average power under pulsed excitation. Figure 6 shows the plot of trapping potential at three chosen average power values for three selected particle sizes. With an increase in laser power, a common trend is observed irrespective of particle size: At low power, the trap is characterized by appearance of a single potential well (PW1) which is first stabilized with increasing power. Then a transition in axial asymmetry is noticed which is followed by appearance of a new potential well (PW2). Further increase in power leads to disappearance of PW1 with concomitant stabilization of PW2. Earlier simulation using dipole approximation also produced the same results [13] except the switch in asymmetry (which is due to interference effects not captured in dipole approximation).

TABLE III. Values corresponds to optimal power, transition behavior, and splitting of potential well for different particle size.

Particle size (nm)	Optimal power (mW)	Power corresponds to transition behavior (mW)	Power corresponds to splitting of potential well (mW)
10	150		2800
20	200	50–100	1700
30	550	130–170	1100
40	1000	200–250	750

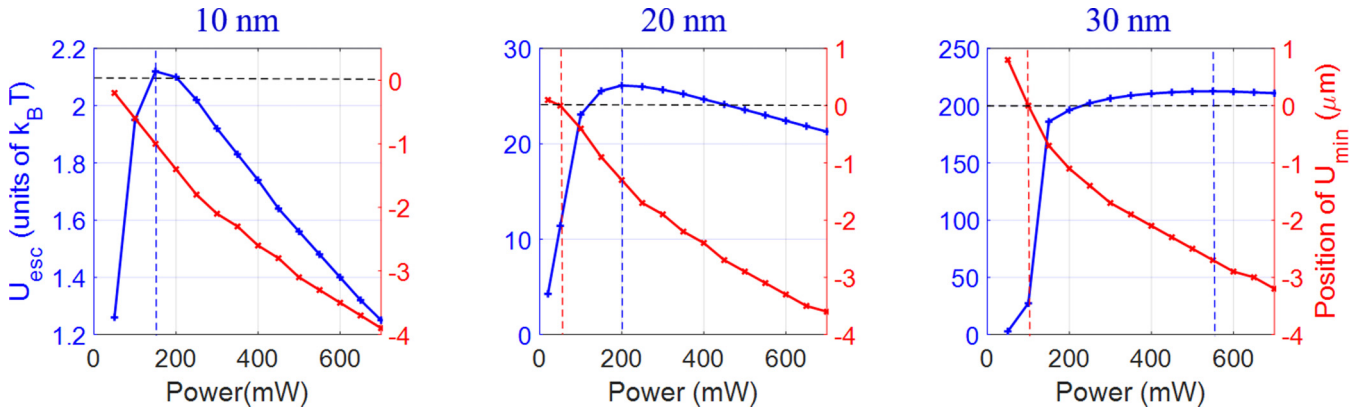

FIG. 7. Plots of escape potential and position of absolute minima against average power using GLMT under pulsed excitation for different particle size.

Quantitative values of optimal power for most stable trap (corresponding to maximum U_{esc}) and power corresponding to switch in axial asymmetry are listed in Table III.

Figure 7 shows escape potential and the position corresponding to potential minimum against average power under pulsed excitation for three selected particle sizes (10, 20, and 30 nm). It can be observed that for 10-nm particle size, the axial asymmetry is always in the negative axial direction, so the position of potential minimum lies behind geometric focus. However, 20- and 30-nm particles initially show axial asymmetry toward positive direction, further increase in average power results in a transition in axial asymmetry. The escape potential on this zero-axial position (when the transition in asymmetry happens, making the potential well symmetric) is $\sim 11\, k_BT$ and $\sim 27 k_BT$ for 20- and 30-nm particle size, respectively. With increasing particle size, the power corresponding to this transition shifts towards higher value. Note that when U_{esc} is maximum (corresponding to most stable trap), the potential minimum lies behind the geometric focus; in other words, for this specific particle size, when laser power is increased the transition in asymmetry happens before the highest value for U_{esc} is attained.

Quite interestingly, contrary to dielectrics [9], the optimal power for most stable trap increases with increasing particle size, as shown in Fig. 8. The noticeable advantage for pulsed excitation is first for any fixed average power the maximum size of the particle to be trapped; for example, at 100-mW average power this limiting size changes from 32 to 34 nm switching from cw to pulsed excitation. Second, this optimal size increases with increasing average power under pulsed excitation whereas it is unchanged under cw excitation (compare Fig. 4). Thus, owing to optical nonlinearity, the limiting particle size can be extended under pulsed excitation.

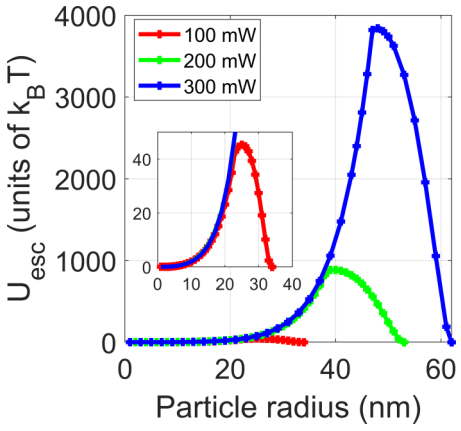

FIG. 8. Plots of escape potential against particle size at different average power under pulsed excitation.

IV. CONCLUSION

In the light of the preceding discussion, we conjecture that even under cw excitation (1064 nm) optical nonlinearity might have played a critical role in earlier experiments on trapping larger-sized (137-nm) particles [6]; inclusion of laser-induced heating (thermal nonlinearity) and hydrodynamic effects is expected to reduce the discrepancy between experiment and theory presented here. Also, the effect of gravity should facilitate trapping of larger particles as they usually have sluggish movement. On the other hand, it should be kept in mind that localized approximation used here should strictly be applicable to smaller-sized particles ($\lambda \gg 2r$) only. Nevertheless, the present work shows how GLMT captures the strong dependence of trapping efficiency on particle size, in particular by reversing the axial asymmetry owing to Fano resonance and how optical nonlinearity further modulates the potential landscape through appearance and disappearance of multiple trapping wells. Most importantly, it explains the origin of existence of the limit for particle size to be trapped and how optical nonlinearity can be harnessed to extend this limit.

ACKNOWLEDGMENTS

This research was supported by the Early Career Research Award from SERB, DST (Grant No. ECR/2016/000467), and by Start-up Grant from IISER Mohali. S.Y. and A.D. acknowledge UGC and IISER Mohali, respectively, for Graduate Fellowships.

The authors declare no competing financial interest.

[1] A. Ashkin, *Optical Trapping and Manipulation of Neutral Particles Using Lasers: A Reprint Volume with Commentaries* (World Scientific, Singapore, 2006).

[2] A. Ashkin, J. M. Dziedzic, J. E. Bjorkholm, and S. Chu, Observation of a single-beam gradient force optical trap for dielectric particles, Opt. Lett. **11**, 288 (1986).

[3] A. Ashkin and J. M. Dziedzic, Optical trapping and manipulation of viruses and bacteria, Science **235**, 1517 (1987).

[4] K. Svoboda and S. M. Block, Optical trapping of metallic Rayleigh particles, Opt. Lett. **19**, 930 (1994).

[5] P. M. Hansen, V. K. Bhatia, N. Harrit, and L. B. Oddershede, Expanding the optical trapping range of gold nanoparticles, Nano Lett. **5**, 1937 (2005).

[6] L. Bosanac, T. Aabo, P. M. Bendix, and L. B. Oddershede, Efficient optical trapping and visualization of silver nanoparticles, Nano Lett. **8**, 1486 (2008).

[7] P. M. Bendix, S. N. S. Reihani, and L. B. Oddershede, Direct measurements of heating by electromagnetically trapped gold nanoparticles on supported lipid bilayers, ACS Nano **4**, 2256 (2010).

[8] A. Lehmuskero, P. Johansson, H. Rubinsztein-Dunlop, L. Tong, and M. Kall, Laser trapping of colloidal metal nanoparticles, ACS Nano **9**, 3453 (2015).

[9] A. Devi and A. K. De, Theoretical investigation on nonlinear optical effect in laser trapping of dielectric nanoparticles with ultrafast pulsed excitation, Opt. Express **24**, 21485 (2016).

[10] A. Devi and A. K. De, Theoretical estimation of nonlinear optical force on dielectric spherical particles of arbitrary size under femtosecond pulsed excitation, Phys. Rev. A **96**, 023856 (2017).

[11] A. Devi and A. K. De, Simultaneous detection of two-photon fluorescence and back-scattered signal of optical trapping of dielectric nanoparticles under femtosecond pulsed excitation, J. Nanophotonics **13**, 020501, (2019).

[12] Y. Jiang, T. Narushima, and H. Okamoto, Nonlinear optical effects in trapping nanoparticles with femtosecond pulses, Nat. Phys. **6**, 1005 (2010).

[13] A. Devi, S. S. Nair, and A. K. De, Disappearance and reappearance of optical trap for silver nanoparticles under femtosecond pulsed excitation: A theoretical investigation, EPL **126**, 28002 (2019).

[14] S. Yadav, A. Devi, and A. K. De, Reversal in axial symmetry of nonlinear optical trapping potential for metallic nanoparticles: generalized Lorenz-Mie theory, Proc. SPIE **11463**, 114632C (2020).

[15] Y. Harada and T. Asakura, Radiation forces on a dielectric sphere in the Rayleigh scattering regime, Opt. Commun. **124**, 529 (1996).

[16] G. Gouesbet, G. Grehan, and B. Maheu, Light scattering from a sphere arbitrarily located in a Gaussian beam, using a Bromwich formulation, J. Opt. Soc. Am. A **5**, 1427 (1988).

[17] G. Gouesbet, G. Grehan, and B. Maheu, Computations of the g_n coefficient in the generalized Lorenz-Mie theory using three different methods, Appl. Opt. **27**, 4874 (1988).

[18] G. Gouesbet, G. Grehan, and B. Maheu, Localized interpretation to compute all the coefficients ${g_n}^m$ in the generalized Lorenz-Mie theory, J. Opt. Soc. Am. A **7**, 998 (1990).

[19] G. Gouesbet and G. Grehan, *Generalized Lorenz-Mie Theory*, (Springer, Berlin, 2011).

[20] M. Dienerowitz, Plasmonic effects upon optical trapping of metal nanoparticles, Ph.D. thesis, 2010, https://research-repository.st-andrews.ac.uk/handle/10023/1634

[21] H. Chen, S. Liu, J. Zi, and Z. Lin, Fano resonance-induced negative optical scattering force on plasmonic nanoparticles, ACS Nano **9**, 1926 (2015).

[22] Y. Yang, J. Li, and Z-Y. Li, Fano resonance of the ultrasensitive optical force excited by Gaussian evanescent field, J. Opt. **17**, 075004, (2015).

[23] K. Liu, X. Xue, V. Sukhotskiy, and E. P. Furlani, Optical Fano resonance in self- assembled magnetic-plasmonic nanostructures, J. Phys. Chem. C **120**, 27555 (2016).

[24] M. F. Limonov, M. V. Rybin, A. N. Poddubny, and Y. S. Kivshar, Fano resonances in photonics, Nat. Photonics **11**, 543 (2017).

[25] M. V. Rybin, K. B. Samusev, I. S. Sinev, G. Semouchin, E. Semouchkina, Y. S. Kivshar, and M. F. Limonov, Mie scattering as a cascade of Fano resonances, Opt. Express **21**, 30107 (2013).

[26] X. Kong and G. Xiao, Fano resonances in core-shell particles with high permittivity covers, in *2016 Progress in Electromagnetic Research Symposium (PIERS)* (IEEE, Piscataway, NJ, 2016), pp. 1715–1719.

[27] M. J. Weber, *CRC Handbook of Optical Material*, Vol. III (CRC Press, Boca Raton, FL, 2003).

[28] D. Rativa, R. E. de Arauno, and A. S. L. Gomes, Nonresonant high-order nonlinear optical properties of silver nanoparticles in aqueous solution, Opt. Express **16**, 19244 (2008).